Thin-Walled Structures 127 (2018) 76–89

Contents lists available at ScienceDirect

Thin-Walled Structures

journal homepage: www.elsevier.com/locate/tws

Full length article

Shear resistance of stiffened steel corrugated shear walls

Jing-Zhong Tong*, Yan-Lin Guo

Department of Civil Engineering, Tsinghua University, Beijing 100084, China

ARTICLE INFO

Keywords:
Steel corrugated shear wall
Stiffener
Shear resistance
Finite element analyses
Transition rigidity ratio
Shear buckling curve

ABSTRACT

In recent years, the steel corrugated shear walls (SCSWs) are widely used in building structures to serve as lateral force resistant members. For some practical engineering applications that the width of the infilled SCSWs in frame structure is much greater than its height, it is common to add vertical stiffening systems to the SCSWs, thus forming the stiffened SCSWs (SSCSWs), and the stiffening system is composed of a pair of vertical stiffeners installed on both sides of the corrugated plate and the connecting high-strength bolts. In this paper, the shear resistant behavior of the SSCSWs is investigated via FE analyses considering both the geometrical and material nonlinearities, and over 300 models are analyzed through elastoplastic numerical process. The comparison of the shear resistant behavior of SSCSWs with different stiffening rigidities is performed, which indicates that the stiffening system can effectively restrain the out-of-plane displacements of the corrugated wall, and can improve both shear resistance and ductility of the SSCSWs. Then a transition rigidity ratio of the stiffening system is proposed to reflect the critical value of the stiffening rigidity that the out-of-plane displacements of the corrugated plate are fully restrained at the bolted locations. Correspondingly, curve fitted formula of the transition rigidity ratio is provided to enable a conservative prediction. Finally, shear buckling formulas are fitted to reveal the relationship between the reduction factor and the normalized aspect ratio, and they are validated to be able to conservatively predict the ultimate shear stress of SSCSWs. Accordingly, some design recommendations are presented, which could provide valuable references for practical design of SSCSWs.

1. Introduction

The lateral force resistant ability of high-rise building is very essential in its design. The lateral force resistance of common frame structures could be significantly improved by adopting steel plate shear walls (SPSWs), and this technique has been utilized in practical engineering structures worldwide. Yet, some disadvantages exist in the frame structures with SPSWs as follows:

(1) Generally, out-of-plane bending rigidities of steel plates are quite small, especially for those with small thickness. Hence, when the SPSW is subjected to lateral forces induced by earthquake or wind effects, it easily buckles and its post-buckling strength would be produced through yielding of the diagonal tension field, leading to a loud noise.
(2) For the structure with its frame and SPSWs installed simultaneously, the vertical loads transmitted from upper structures would be applied to the SPSWs, thus producing pre-compression and influencing the shear resistance of the SPSWs [1].

With those considerations, the infilled steel plates could commonly be replaced by steel corrugated plates, forming the steel corrugated shear walls (SCSWs). Numerous investigations were conducted by researchers to perform the comparison of the shear resistance and hysteretic behavior between SPSWs and SCSWs [2–6]. Berman et al. [2,3] performed the comparison of hysteretic performances among SPSWs, ordinary concentrically braced frames (OCBFs) and SCSWs, in which the corrugations were set in a diagonal direction with an inclination angle of about 45°. Emami et al. [4,5] conducted hysteretic tests of SPSWs and SCSWs, in which the corrugations installed horizontally and vertically were respectively considered. Kalai et al. [6] conducted FE analyses of SPSWs and SCSWs under cyclic shear loads to perform comparison, in which the effect of corrugation shapes on the hysteretic performances of SCSWs was investigated. According to these researches, by utilizing SCSWs in frame structures, the shear buckling loads could be significantly promoted owing to the increase of bending rigidities of the steel corrugated plates. In addition, based on the investigations performed by Tong and Guo [7], the vertical pre-compression loads could be efficiently released for the SCSWs with their corrugations laid horizontally. Due to these advantages of SCSWs, they have been widely used in practical building structures as lateral force resistance systems in recent years, as shown in Fig. 1. Current

* Corresponding author.
E-mail addresses: tjz13@mails.tsinghua.edu.cn (J.-Z. Tong), gyl@tsinghua.edu.cn (Y.-L. Guo).

https://doi.org/10.1016/j.tws.2018.01.036
Received 3 October 2017; Received in revised form 21 November 2017; Accepted 24 January 2018

Nomenclature

a	amplitude of the corrugation
A_a	cross-sectional area of single steel angle stiffener
b	width of the steel corrugated shear wall
b_0	location of neutral axis of single steel angle stiffener
b_a	width of the steel angle stiffener
d_1,d_2	dimensions of the corrugation
D_x,D_y,D_{xy},H	rigidity constants of equivalent orthotropic plate
E	Young's modulus of steel
h	height of the steel corrugated shear wall
I_a	moment of inertia of single steel angle stiffener
I_s	Equivalent moment of inertia of the stiffening system
k	elastic buckling coefficient
k_1	elastic buckling coefficient of 1-side fixed, 3-side simply-supported orthotropic plate
k_2	elastic buckling coefficient of 2-side fixed, 2-side simply-supported orthotropic plate
q	arc length of one repeating corrugation
t	thickness of the steel corrugated shear wall
t_a	thickness of the steel angle stiffener
V	lateral shear load
β	converted aspect ratio of the steel corrugated shear wall
γ	angle of the incline segment in the corrugation
δ	lateral displacement of the steel corrugated shear wall
η	rigidity ratio of the stiffening system
$\eta_{0,e}$	transition rigidity ratios under elastic buckling analyses
$\eta_{0,p}$	transition rigidity ratios under elastoplastic analyses
θ	constant of equivalent orthotropic plate
λ	wave length of one repeating corrugation
λ_n	normalized aspect ratio of the stiffened steel corrugated shear wall
τ	shear stress
τ_{cr}	shear elastic buckling stress
τ_u	shear ultimate stress
τ_y	shear yield stress
υ	Poisson's ratio of steel
φ	reduction factor
φ_{lim}	upper limit of the reduction factor
Φ	intermediate variable of the reduction factor

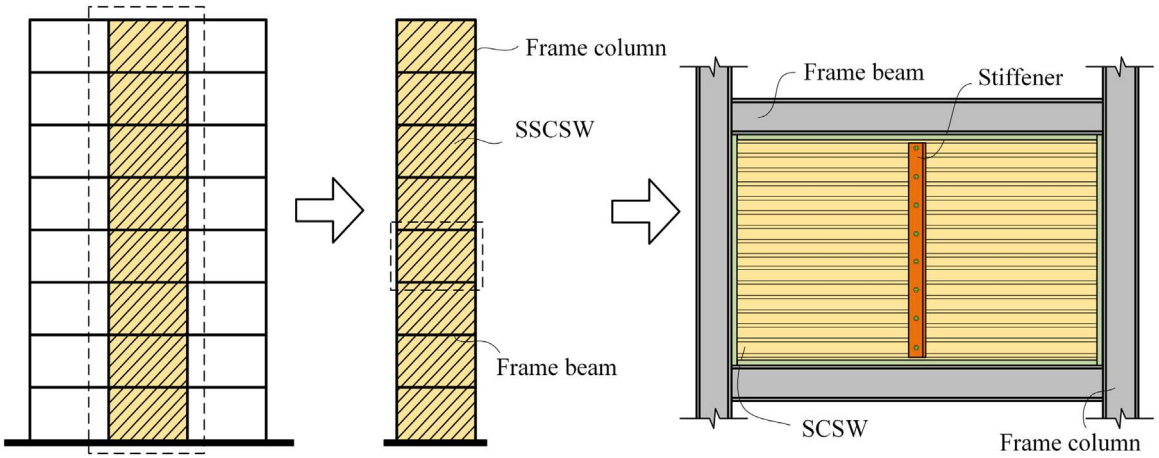

Fig. 1. SSCSWs in frame structures.

researches on SCSWs mainly focused on the shear resistance of SCSWs with small thickness (i.e. $t = 0.5 - 1.5$mm), and numerous experimental and numerical investigations have been published [8–16]. The SCSWs with small thickness are easily to be profiled into trapezoidal corrugations. However, they are only suitable for the applications in low-rise buildings since the thickness of SCSWs inevitably limits their upper bound of shear resistance. In order for the applications of corrugated plates with small thickness in high-rise buildings, multiple corrugated plates would be required to improve the ultimate resistance. Otherwise, SCSWs with large thickness (i.e. $t = 4 - 8$mm) should be adopted in high-rise buildings, which benefited from both the improvements of the steel ductile properties and the equipment for cold rolling. Correspondingly, the shear resistant behavior of SCSWs with large thickness is worth of investigation for high-rise structural applications.

In some practical structures, especially for long-span frame structure applications, the width of the SCSW is much greater than its height. In these situations, the shear resistance of the SCSW could be remarkably improved by adding a vertical stiffening system to it, thus forming the stiffened SCSWs (SSCSWs) as depicted in Fig. 1. For convenience of connections between the SCSW and stiffeners, the corrugations are usually chosen to be trapezoidal shapes, and the most commonly used types of corrugation shapes are depicted in Fig. 2. Among these shapes, the first type is the most adopted and it is therefore selected in the following discussions of this paper.

On the shear resistant behavior of SSCSW, little researches have been presented and the design method of shear resistance is of great concern of the engineers. The shear elastic buckling behavior of SSCSWs has been studied by the authors and formulas for shear elastic buckling loads were proposed [7]. On this basis, this paper would present the shear resistant behavior and corresponding design method of SSCSWs via FE nonlinear analyses.

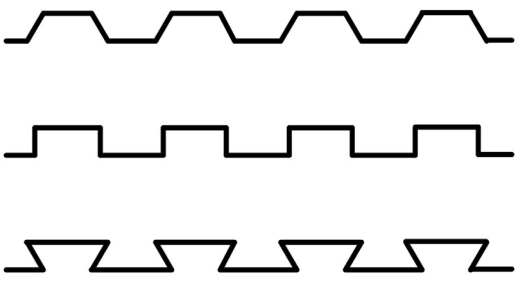

Fig. 2. Shapes of corrugations.

2. Construction details and elastic buckling of SSCSWs

2.1. Connection details and boundary conditions

As mentioned above, the corrugations in the SSCSW are usually laid horizontally to release the vertical pre-compression, as shown in Fig. 3, and the stiffening system is vertically installed. The stiffening system is composed of a pair of stiffeners placed on both sides of the corrugated plate and the connecting bolts. The stiffeners could be selected as steel angles, steel channels, rectangular tubes or other sections. It is assumed that the main function of the stiffeners are to provide additional out-of-plane constraints to the corrugated plate, thus the contribution of their flexural rigidity is only involved in the FE analyses. The behavior of stiffeners and their design methods are out of major concern of this paper. Hence, steel angles are adopted as stiffeners in the following discussions. The vertical stiffeners are connected with the corrugated plate with bolts in which either ordinary or high-strength bolts could be selected. Yet for some SSCSWs with small thickness, ordinary bolt connections may easily lead to local fracture of the corrugated plate near the bolted regions. Thus, high-strength bolts with pre-tightening forces are recommended for practical engineering, especially for some applications of corrugated plates with small thickness, to enable tightening contact along stiffener/plate interfaces and to avoid local fracture of the corrugated plate. Since a single column of high-strength bolts is only installed, as shown in Fig. 3, the rotational constraints about the column provided by the stiffening system to the SCSW is negligible. In addition, by adopting the open-sectional steel angles as stiffeners, it is convenient to accomplish the double-sided bolted connections during practical construction process.

Additionally as depicted in Fig. 3, the corrugated plate in the SSCSW is connected with surrounding frame beams and columns with connecting transition components: the corrugated plate is connected with the frame beams with fish plates (A-A sectional view in Fig. 3), while it is connected with the frame columns with connecting steel channels (B-B sectional view in Fig. 3). The connecting transition components, including fish plates and steel channels, are both welded onto the edges of the SSCSW when fabricated in manufacturers, and during construction process on site, these connecting transition components are further welded with the surrounding frame members. By adopting the connecting transition components, the out-of-plane rigidity of the SSCSW could be significantly improved because these components behave like edge stiffeners, hence controlling occurrence of large out-of-plane deflections of the SSCSW during its transportation and erection. Since bending moment could be transmitted via connecting steel channels yet it could not be transmitted via fish plates, the boundary conditions of the SSCSW could be regarded to be 2-side fixed and 2-side simply-supported, as shown in Fig. 4.

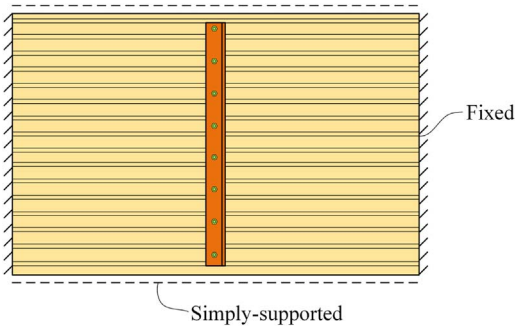

Fig. 4. Boundary conditions of SSCSWs.

2.2. Buckling modes

In SSCSWs, the infilled corrugated plate is divided by the vertical stiffening system into sub-panels, and hence three different types of buckling modes might occur in both elastic and elastoplastic conditions. Firstly, the corrugated plate can be regarded as an assembly of a series of narrow plates, and local buckling would inevitably occur when the

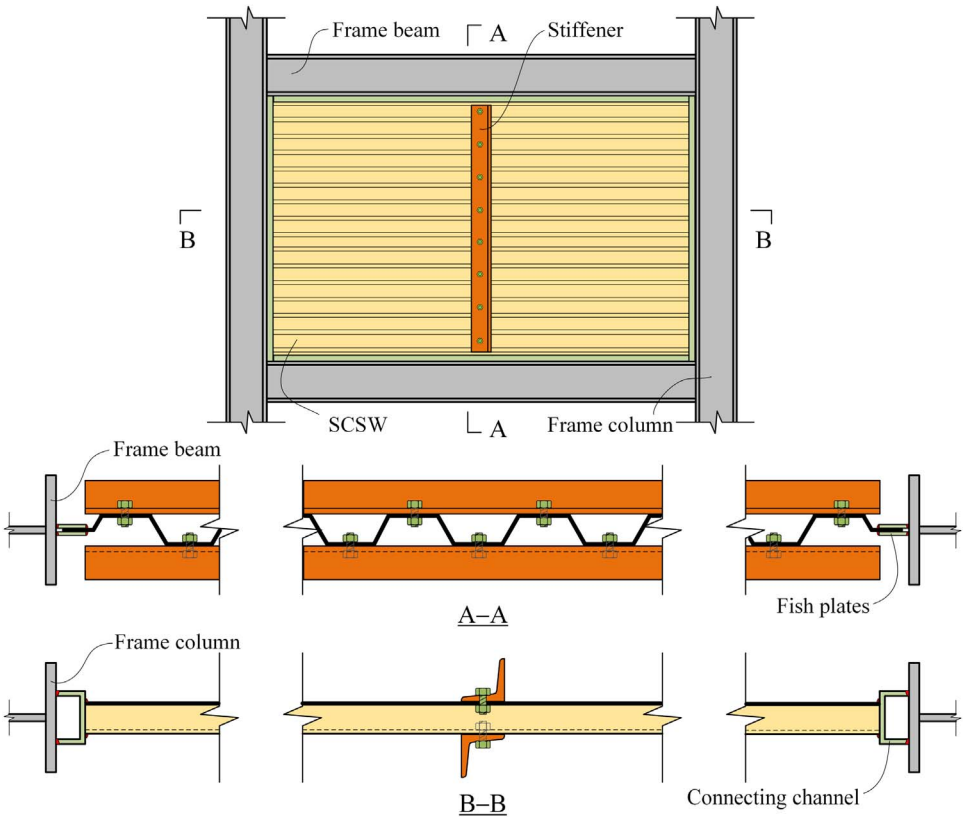

Fig. 3. Connection details of SSCSWs.

width-to-thickness ratio of these narrow plates gets too large, exhibiting a buckling mode that the buckling waves are occurred separately within the narrow plates, as shown in Fig. 5(a). When designing SSCSWs, local buckling mode could be effectively prevented by choosing appropriate corrugation parameters; for the SSCSWs with larger thickness, the width-to-thickness ratio of the narrow plates gets smaller and the local buckling mode is less likely to occur. Secondly, when the flexural rigidity of the stiffening system is quite small and it could not provide adequate out-of-plane displacement constraints, global buckling would occur, exhibiting several diagonal buckling waves across the vertical stiffening system, as shown in Fig. 5(b). Thirdly, sub-panel buckling would occur when the flexural rigidity of the stiffening system gets large enough. In this situation, the out-of-plane displacements of the infilled SCSW are fully restrained at the bolted locations, and the overall buckling waves are divided by the stiffening system and occur within each of the sub-panels.

In this paper, the local buckling mode is prevented by choosing appropriate design parameters, which is also recommended for practical structural engineering. The global buckling and sub-panel buckling modes are of major concern and would be discussed in the following sections.

2.3. Shear elastic buckling loads of SSCSWs

Formulas of shear elastic buckling loads are of significance for practical design of SSCSWs. The post-buckling strength of SCSW is commonly negligible since the diagonal tension field is difficult to form. Hence, for a thin SSCSW, the elastic buckling load could approximately represent the shear resistance. In addition, for a thick SSCSW the formulas of elastic buckling load is essential in calculating the normalized aspect ratio, which is a key parameter in elastoplastic design of SSCSWs.

The shear buckling formulas of SCSWs were firstly proposed in 1970s [17,18], and recently some researchers provided some extended investigations on elastic buckling behavior of SCSWs [19–21]. In these researches, the SCSW was considered equivalent as an orthotropic plate, as shown in Fig. 6, and the rigidity constants, D_x, D_y and H, of the equivalent orthotropic plate could be expressed as

$$D_x = \frac{E}{\lambda}\cdot\left(2d_1 ta^2 + \frac{4ta^3}{3\sin\gamma}\right),\ D_y = \frac{\lambda}{q}\cdot\frac{Et^3}{12(1-\upsilon^2)},\ H = \frac{1}{2}D_{xy} = \frac{q}{\lambda}\cdot\frac{Et^3}{12(1+\upsilon)} \tag{1}$$

in which E and υ are respectively the Young's modulus and Poisson's ratio of the material;

t is the thickness of the corrugated plate; and other geometrical parameters of the corrugation, including d_1, d_2, a, γ, λ and q, are depicted in Fig. 6(b). For different types of corrugated plates with different geometrical dimensions, the rigidity constants D_y and H are generally in the same order of magnitude while the rigidity constant D_x is commonly two orders of magnitude higher than them.

In order to better describe the shear resistant behavior of the orthotropic plate, two converted parameters were introduced by Easley [18] as

$$\theta = \frac{H}{\sqrt{D_x D_y}} \tag{2}$$

$$\beta = \frac{b}{h}\cdot\left(\frac{D_y}{D_x}\right)^{1/4} \tag{3}$$

in which θ represents the ratio between twisting and bending rigidities of the equivalent orthotropic plate; for steel plate, this parameter could be calculated as $\theta = 1.0$, while for corrugated plates, the value of θ is commonly less than 0.2. In addition, b and h are respectively the width and height of the equivalent orthotropic plate, and β is the converted aspect ratio of the equivalent orthotropic plate.

On these basis, shear elastic buckling formula of SCSWs was provided [18] as

$$\tau_{cr} = k\cdot\frac{D_x^{3/4}D_y^{1/4}}{t\cdot b^2} \tag{4}$$

in which τ_{cr} is the shear elastic buckling stress of the orthotropic plate, and k is the elastic buckling coefficient.

This formula of Eq. (4) has been proved to be able to well predict the shear elastic buckling stress of ordinary SCSWs (without stiffening systems). However, calculation of the elastic buckling loads of SSCSWs is much more complicated, since the flexural rigidity of the stiffening system should be taken into consideration. As shown in Fig. 7(a), the steel angle stiffeners installed on both sides of the corrugated plate are connected with the plate via high-strength bolts, and the stiffening system and corrugated plate would bend together without much slippage along their interfaces. Especially for situations with thick corrugated plate, in which the rigidity of the corrugated plate segment between adjacent bolts are quite large, the stiffening system along with the corrugated plate could be regarded as a truss member. Hence, as depicted in Fig. 7(b), the flexural rigidity of the stiffening system should be calculated by considering the whole section of two steel angle stiffeners as

$$EI_s = 2EI_a + 2EA_a\cdot(a + b_0)^2 \tag{5}$$

in which I_s is the equivalent moment of inertia of the stiffening system; I_a and A_a are respectively the moment of inertia and cross-sectional area of single steel angle stiffener; b_0 represents the location of neutral axis of single steel angle stiffener, as shown in Fig. 7(b).

Accordingly, a parameter of rigidity ratio η could be defined by Eq. (6) [7], representing the ratio of flexural rigidities between the stiffening system and the corrugated plate. This non-dimensionalized parameter was proposed to describe the restraining effect of the stiffening system on the corrugated plate, and it would be a key parameter for the SSCSW design.

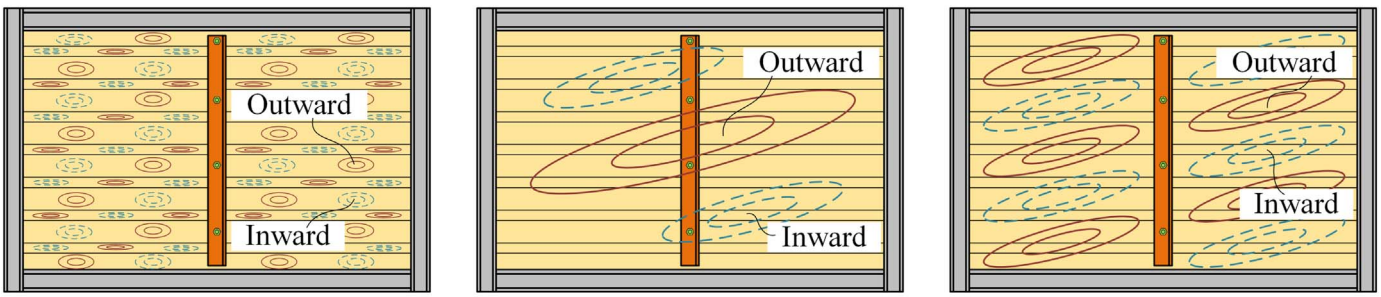

Fig. 5. Buckling modes of SSCSWs.

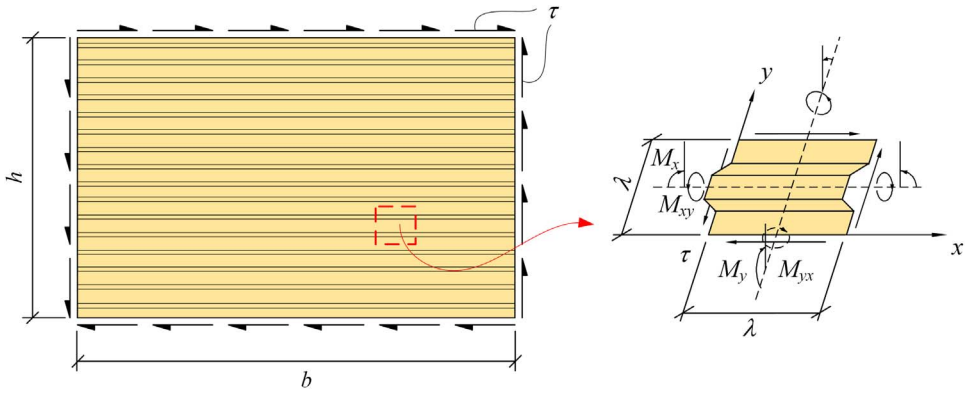

(a) Orthotropic model of SCSW and its Isolated element

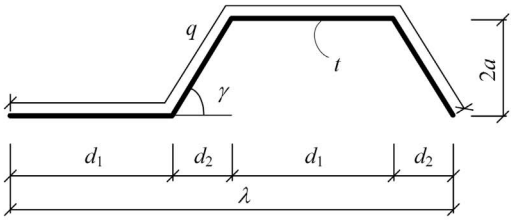

(b) Geometric parameters of corrugation

Fig. 6. Equivalent orthotropic model and geometrical parameters of SCSWs.

$$\eta = \frac{2EI_s}{D_y b} \tag{6}$$

Based on the authors' previous investigations about shear elastic buckling formulas of SSCSWs [7], when the flexural rigidity of the stiffening system is negligible ($\eta = 0$), the SSCSW returns back to an ordinary SCSW without stiffening system and its boundary conditions could be regarded as 2-side fixed, 2-side simply-supported, as shown in Fig. 8. On the other hand, when the flexural rigidity of the stiffening system gets large enough and exceeds the transition rigidity ratio ($\eta > \eta_{0,e}$), the out-of-plane displacements of the corrugated plate at the bolted locations are fully restrained, and hence the SSCSW could be simplified into a half structure of the ordinary SCSW with 1-side fixed, 3-side simply-supported, as shown in Fig. 8.

It was previously proved by the authors [7] that Eq. (4) could be adopted to well predict the shear elastic buckling loads of SSCSWs, and the elastic buckling coefficient k should be calculated in terms of the value of η, as depicted in Fig. 9. Based on the previous discussions, if $\eta = 0$, k equals to the elastic buckling coefficient of the 2-side fixed, 2-side simply supported corrugated plate, denoted by k_2 and expressed by Eq. (8) [7]. If η exceeds the transition rigidity ratio, i.e. $\eta > \eta_{0,e}$, k equals to the elastic buckling coefficient of the 1-side fixed, 3-side simplified supported corrugated plate, denoted by k_1 and expressed by Eq. (7) [7]; since the original corrugated plate is simplified into half structure in this situation, a magnification factor of 4 should be introduced, i.e. $k = 4k_1$.

$$k_1 = (7 + 20\theta)\cdot\beta^2 + 8\beta + 45 + 25\theta \tag{7}$$

$$k_2 = (7 + 20\theta)\cdot\beta^2 + 8\beta + 61.2 + 29.5\theta \tag{8}$$

In investigations presented in [7], by utilizing the theorem of minimum potential energy and the Ritz method, the elastic buckling coefficient of SSCSWs could be expressed as

$$k = \begin{cases} k_2 + (4\,k_1 - k_2)\cdot\sqrt{1 - (1 - \eta/\eta_{0,e})^{1.7}} & \eta \le \eta_{0,e} \\ 4k_1 & \eta > \eta_{0,e} \end{cases} \tag{9}$$

in which $\eta_{0,e}$ is the transition rigidity ratio under elastic buckling

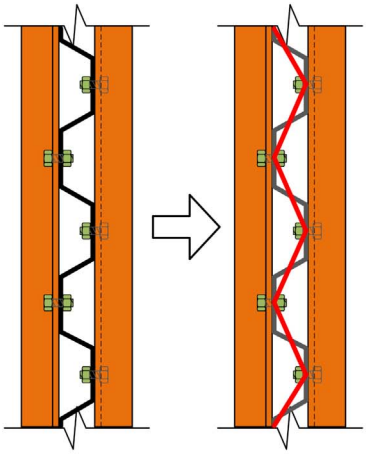

(a) Truss effect of the stiffening system

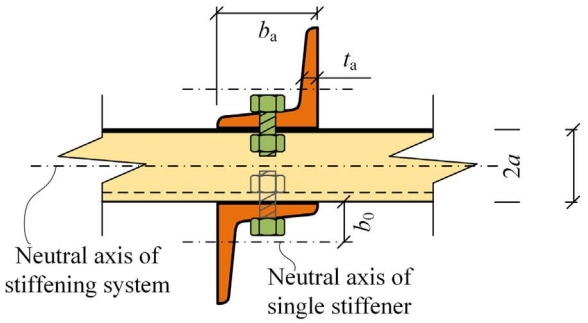

(b) Flexural rigidity of the stiffening system

Fig. 7. Flexural rigidity of the stiffening system.

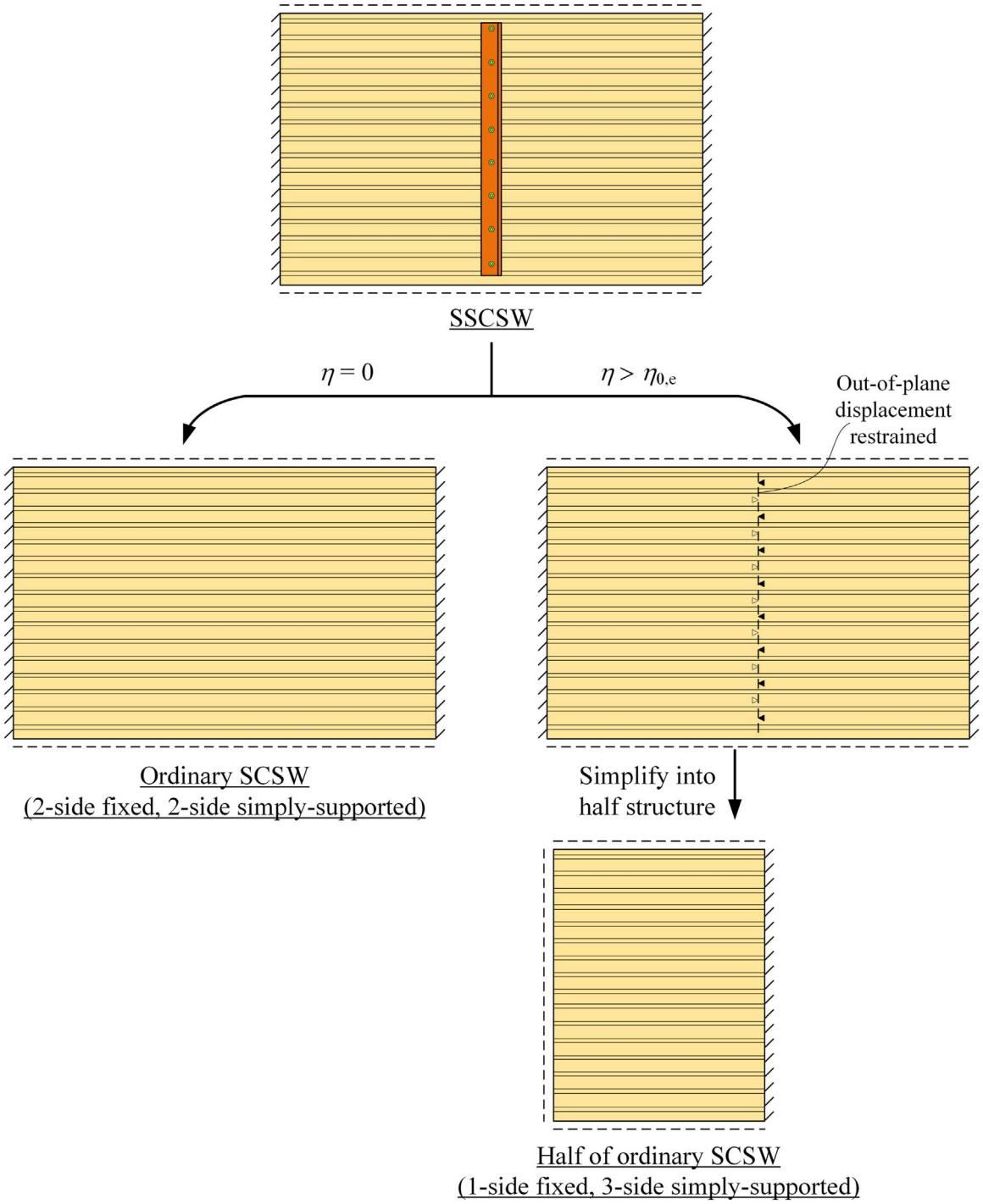

Fig. 8. Elastic buckling models with different rigidity ratios.

analyses and an approximate value of $\eta_{0,e} = 100$ was proposed in [7] and was validated to be reasonable for most of the SSCSW cases without much discrepancy.

3. Finite element model of SSCSWs

The construction details and elastic buckling behavior of SSCSWs have been introduced in the previous sections. In the following discussions, the shear resistance of the SSCSWs would be investigated via FE numerical analyses, in which both the geometrical and material nonlinearities are taken into consideration. As depicted in Fig. 10, FE models are constructed via ANSYS. In each of the models, the infilled corrugated plate and the surrounding frame members are modelled by 4-node shell elements with six degrees of freedom at each node, while the vertical stiffeners are modelled by beam elements with six degrees of freedom at each node. The Young's modulus of the infilled corrugated plate and stiffeners are set to be $E = 206$GPa, and the frame beams and columns are set to be infinitely rigid to eliminate the effect of the frame member deformations on the shear resistance behavior of the infilled plate. The material properties of the infilled corrugated plate and stiffeners are both set to be ideally elastoplastic and their yield stress are taken respectively as 235MPa and 345MPa by referring to the material properties specified in the Chinese code for design of steel structures [22].

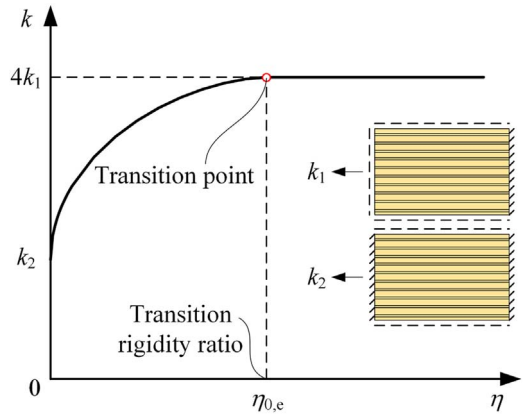

Fig. 9. Transition rigidity ratio of SSCSWs under elastic buckling analyses.

In addition, as shown in Fig. 10(a), the joints between frame beams and column are set to be hinged to eliminate their contributions to resist lateral forces. Since the connecting transition components, including the fish plates and connecting steel channels, are only installed for connecting transition utilizations, they are not modelled in the FE modelled. In order to simulate the high-strength bolt connections between the corrugated wall and stiffeners, the three translational displacement components of the nodes in the bolted locations are coupled. For simplicity of the FE models, the contact behavior along the corrugated wall/stiffener interfaces are ignored. Since the contact effects produced by the stiffeners would provide additional out-of-plane constraints to the corrugated wall, the FE model without considering the contact effects would produce a conservative prediction of the ultimate shear resistance of the SSCSW and lead to a safe design. The rotations of the vertical stiffeners about their central axes are restrained to eliminate their rigid body displacements. An in-plane shear force τ is applied to the top frame beam of the SSCSW. Moreover, the corrugation dimensions adopted in the FE models are shown in Fig. 10(b), which refers to a shape of corrugation that has been utilized in practical engineering structures [23], and the thickness of the corrugated wall is also set in a range of $t = 4 - 8$mm by referring to the practical applications. As is known that the shape of corrugations would significantly influence the shear-carrying behavior of the SSCSWs. For instance, when the amplitude of the corrugation a is quite small, the corrugate plate behaves quite similar to a flat plate under in-plane shear loads; when a is large, more features of corrugated plates would be exhibited. As is mentioned in the previous sections that θ is a highly representative parameter in describing the behavior of corrugated plate by introducing the orthotropic plate model. The value of θ is closely related to both the corrugation shape and thickness of the corrugated plate; $\theta = 1.0$ could be calculated from ordinary flat steel plates, while $\theta < 0.2$ is satisfied for commonly utilized corrugated plates. Among the models involved in this paper, the parameter lies in a range of $0.08 < \theta < 0.16$, which could be regarded as the parameter range for applications of the conclusions drawn from the following parametric analysis. Fig. 10(c) depicts the meshing size of the FE models.

4. Shear resistant behavior of SSCSWs

4.1. FE elastoplastic analyses

By means of the constructed FE models introduced in the previous section, the shear resistant behavior of SSCSWs would be investigated via FE elastoplastic analyses in this section. The model details are tabulated in Table 1, the heights of the corrugated plates are all set to be 2100mm. Among these models, three cases, with the corrugated plate thickness of $t = 4$mm, 6mm and 8mm respectively, are involved in order to cover the commonly used thickness range of the SSCSWs. In each of the cases, five different overall dimensions of corrugated plates with their aspect ratios of $b/h = 1.0$, 1.5, 2.0, 2.5 and 3.0 respectively, are included, which are considered to cover the practical range of aspect

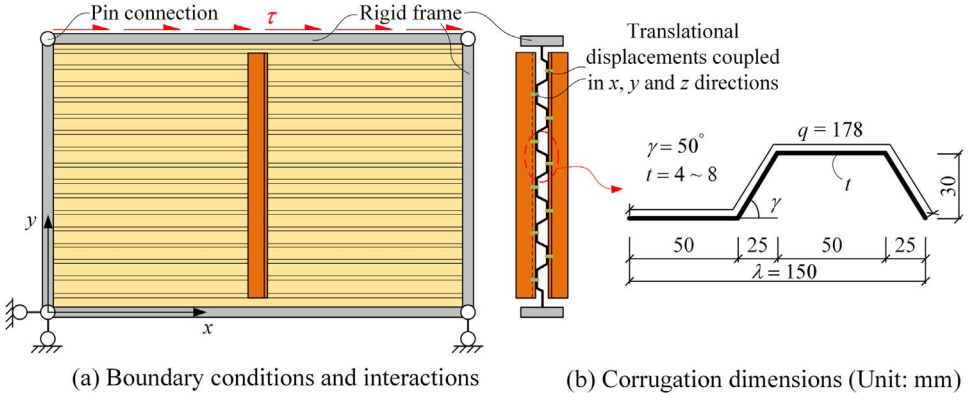

(a) Boundary conditions and interactions (b) Corrugation dimensions (Unit: mm)

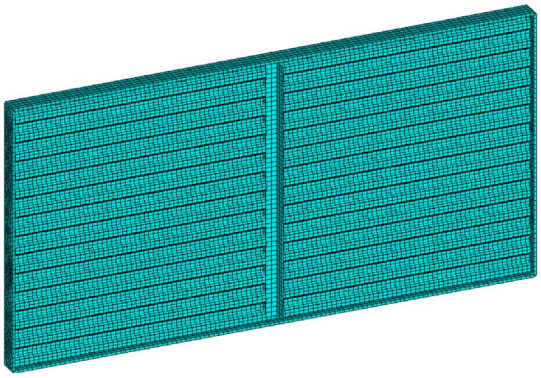

(c) FE model and meshing size

Fig. 10. FE model for nonlinear analyses.

Table 1
FE model details.

Model		Geometrical parameters					Design parameters					FE results		
Case	Label	t (mm)	h (mm)	b (mm)	$\frac{b}{h}$	Steel angle[a] ($b_a \times t_a$, mm)	θ	η	β	k	λ_n	φ	φ_{lim}	$\eta_{0,p}$
1	Case-1–1.0	4	2100	2100	1.0	0 × 0-47 × 6	0.080	0–220	0.284	66–200	0.520-0.901	0.877–0.979	1.000	9
	Case − 1 to 1.5			3150	1.5	0 × 0-50 × 8			0.426	68–208	0.765-1.332	0.584–0.961	0.976	71
	Case − 1 to 2.0			4200	2.0	0 × 0-60 × 7			0.568	71–217	0.998-1.747	0.444–0.794	0.804	162
	Case − 1 to 2.5			5250	2.5	0 × 0-65 × 7			0.711	74–228	1.217-2.143	0.382–0.613	0.641	195
	Case − 1 to 3.0			6300	3.0	0 × 0-68 × 8			0.853	77–240	1.423-2.520	0.348–0.528	0.550	208
2	Case-2–1.0	6	2100	2100	1.0	0 × 0-80 × 6	0.120	0–220	0.348	69–208	0.461-0.802	0.930–0.978	1.000	3
	Case-2–1.5			3150	1.5	0 × 0-80 × 9			0.522	72–219	0.674-1.179	0.696–0.979	1.000	26
	Case-2–2.0			4200	2.0	0 × 0-90 × 9			0.696	75–232	0.871-1.536	0.555–0.878	0.894	117
	Case − 2 to 2.5			5250	2.5	0 × 0-95 × 9			0.870	79–248	1.054-1.871	0.483–0.738	0.775	157
	Case − 2 to 3.0			6300	3.0	0 × 0-100 × 10			1.044	83–266	1.221-2.183	0.446–0.653	0.684	135
3	Case-3–1.0	8	2100	2100	1.0	0 × 0-100 × 9	0.159	0–220	0.402	71–215	0.421-0.735	0.965–1.000	1.000	0
	Case-3–1.5			3150	1.5	0 × 0-108 × 10			0.603	74–230	0.611-1.075	0.791–0.991	1.000	7
	Case-3–2.0			4200	2.0	0 × 0-120 × 11			0.804	79–248	0.785-1.392	0.645–0.929	0.944	53
	Case-3–2.5			5250	2.5	0 × 0-130 × 11			1.005	84–269	0.942-1.684	0.573–0.827	0.851	82
	Case-3–3.0			6300	3.0	0 × 0-130 × 12			1.206	90–294	1.082-1.951	0.531–0.755	0.790	105

[a] The angle size of 0 × 0 represents the ordinary SCSW without vertical stiffeners.

ratios. Hence, a total of fifteen groups of models is involved in the FE analyses. In each of the groups, there are variations in the flexural rigidities of the stiffening systems by changing the steel angle stiffener dimensions, and correspondingly, the rigidity ratio values are in a range of $\eta = 0 - 220$ to study the effect of the stiffening rigidities on the shear resistance of the SSCSWs.

In total, numerical results of over 300 FE elastoplastic models are involved in this section. In order to provide better understanding of the shear elastoplastic buckling behavior of SSCSWs, a parameter of normalized aspect ratio is defined as

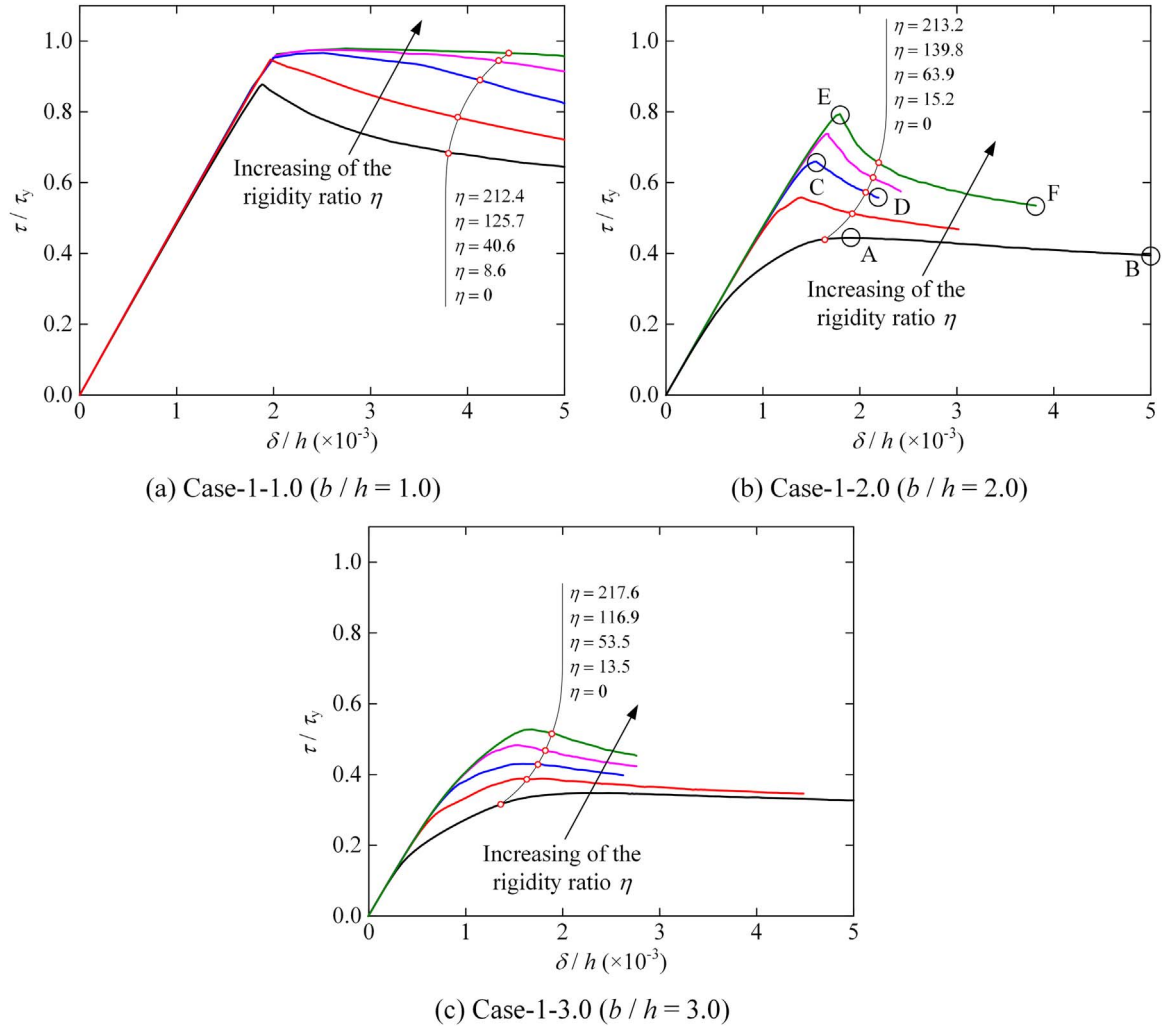

Fig. 11. Shear stress versus lateral displacement curves of FE models.

$$\lambda_n = \sqrt{\frac{\tau_y}{\tau_{cr}}} \tag{10}$$

in which τ_y is the shear yield stress of the steel material, and τ_{cr} is the shear elastic buckling stress calculated from Eqs. (4) and (9). As a key parameter for shear resistant design of SSCSWs, the λ_n values of each model group are also calculated and tabulated in Table 1.

In order to compare the models with different rigidities of the stiffening systems, Fig. 11 depicts the shear stress versus lateral displacement curves of SSCSWs with different rigidity ratios, in which three model groups of Case-1 with aspect ratios of b/h = 1.0, 2.0 and 3.0 respectively are involved. The y-axis of the figures is the lateral shear load τ normalized by the yield shear stress τ_y, hence all of the curves are below the horizontal line of 1.0. The x-axis is the storey drift angle of the SSCSW, denoted by δ/h. As shown in Fig. 11, for the same aspect ratio of the corrugated plate, the shear resistance of SSCSW would be improved with the increase of stiffening rigidity. Moreover, as depicted in Fig. 11(a) corresponding to Case-1–1.0, when the stiffening rigidity changes from $\eta = 0$ to $\eta = 8.6$, the shear resistance of SSCSW increases remarkably. When the rigidity ratio increases continuously, the ultimate load of the SSCSW does not increase anymore, however, the ductility can still be improved with the increase of the stiffening rigidity. This indicates that adding stiffening systems to the ordinary SCSWs can improve both their shear resistance and ductility.

It is observed from Fig. 11 that the tendencies of the curves vary. For some of them, a sudden drop occurs in the shear resistance right after the ultimate resistance is achieved, as those shown in Fig. 11(b); while for others, the shear resistance decreases gradually after the ultimate resistance is achieved, as those shown in Fig. 11(c). Based on the observations of FE results, the sudden drop in curves is caused by the sudden fracture of the stiffeners with large deflections and hence the corrugated plate loses its out-of-plane supports. In contrast for the model without significant stiffener deflections (or the SCSW models without stiffeners), the shear resistance decreases gradually after the ultimate resistance is achieved.

Moreover, during the FE elastoplastic analyses of the SSCSWs, three typical failure modes are observed:

(1) When the aspect ratio is quite small or thickness is quite large (e.g. b/h = 1.0 shown in Fig. 11(a)), the SSCSW yields before significant out-of-plane deflections of the corrugated plate occur, thus little deformation could be observed in the stiffeners; hence, the shear resistance of SSCSW would decrease gradually after the ultimate resistance is achieved.
(2) When the aspect ratio gets larger (e.g. b/h = 2.0 shown in Fig. 11(b)), the SSCSW fractures with significant out-of-plane deflections across the whole panel (similar to the global buckling mode depicted in Fig. 5(b)), and significant out-of-plane deformation could be observed in the stiffeners; hence, sudden drops in the curves of Fig. 11(b) are observed.
(3) For the SSCSWs with quite large aspect ratios (e.g. b/h = 3.0 shown in Fig. 11(c)), the out-of-plane rigidity of the corrugated plate becomes relatively small. These SSCSWs commonly fracture with out-of-plane deflections within the sub-panels (similar to the sub-panel buckling mode depicted in Fig. 5(c)), thus little deformation could be observed in the stiffeners; hence, the shear resistance of SSCSW would decrease gradually after the ultimate resistance is achieved.

These load-carrying behaviors described above could well coincide with the features shown in the curves of Fig. 11. It is recognized that the load-carrying behavior of the SSCSWs is closely related to both the behavior of the corrugated plate and stiffeners. In order to provide better understanding of the shear resistant behavior of the SSCSWs, the displacement and stress distributions of typical FE models would be discussed by introducing three models of Case-1–2.0 with different rigidity ratios. As shown in Fig. 12, a model with $\eta = 0$ (ordinary SCSW

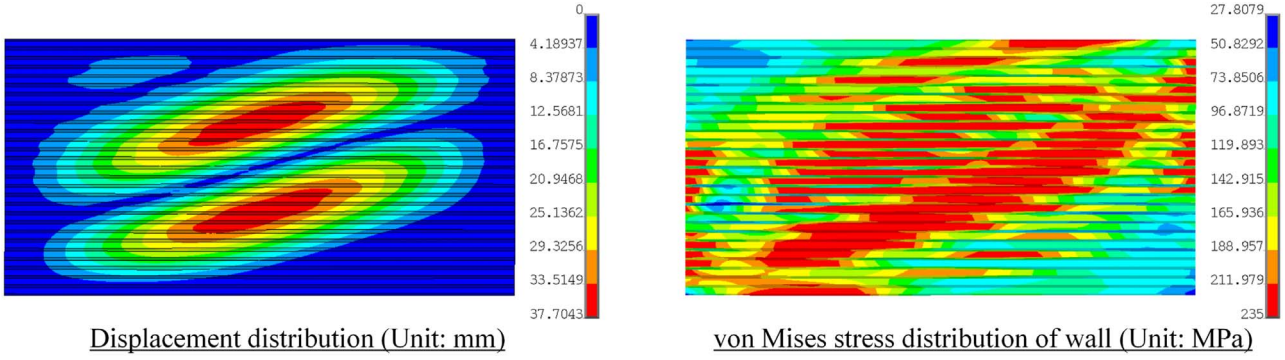

Fig. 12. Displacement and stress distributions of Case-1–2.0 (η = 0).

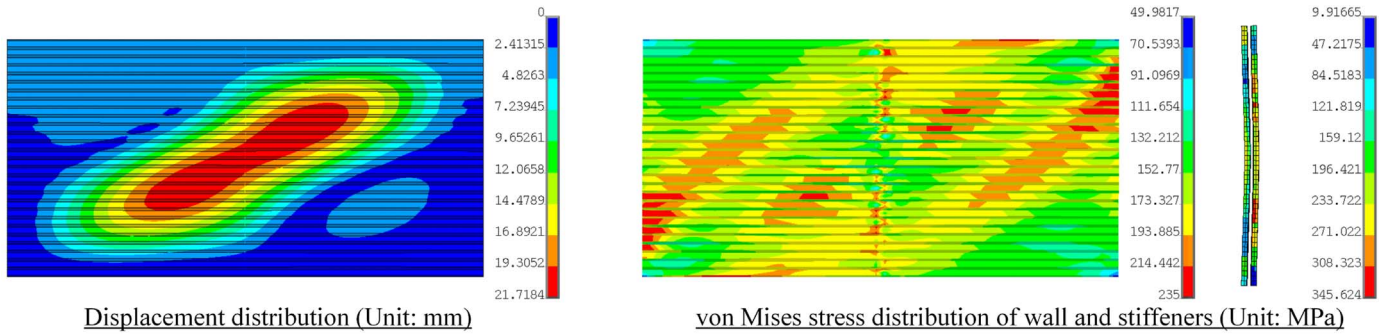

(a) Ultimate state (Point C in Fig. 11)

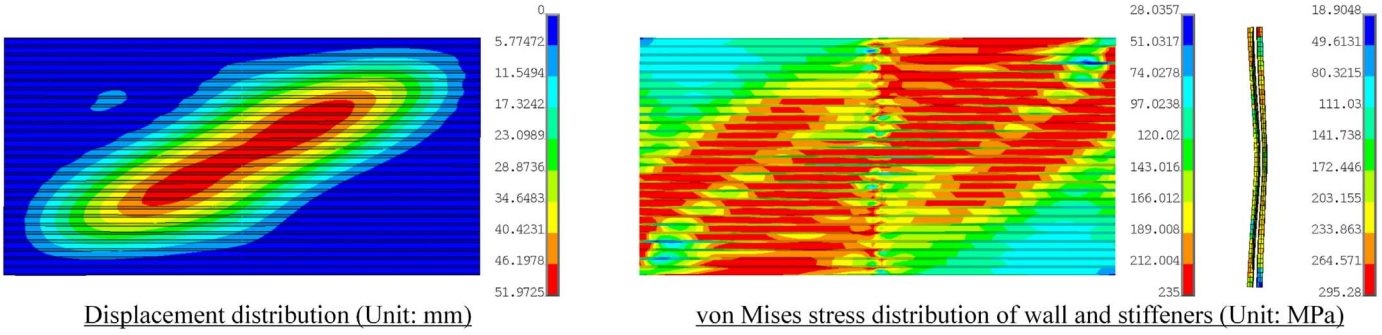

(b) Final state (Point D in Fig. 11)

Fig. 13. Displacement and stress distributions of Case-1–2.0 (η = 63.9).

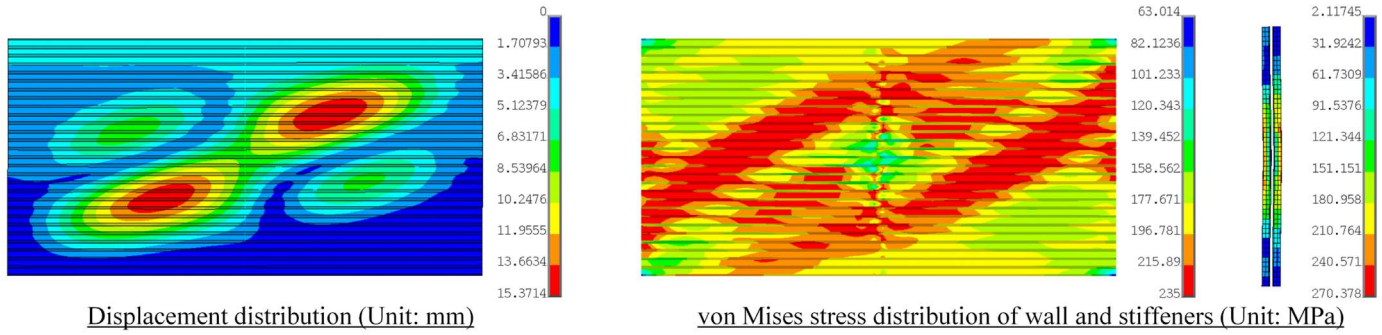

(a) Ultimate state (Point E in Fig. 11)

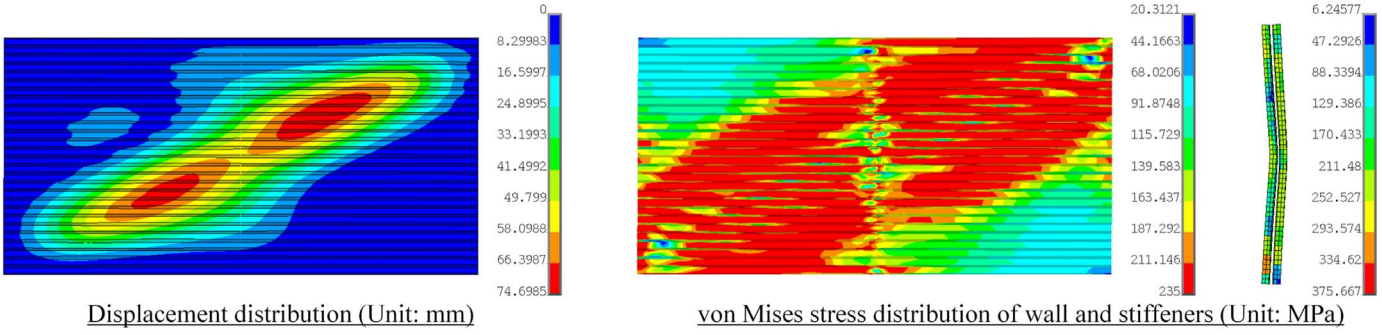

(b) Final state (Point F in Fig. 11)

Fig. 14. Displacement and stress distributions of Case-1–2.0 (η = 213.2).

without stiffening system) is presented. It is observed that the buckling waves of the SCSW lay diagonally across the whole wall and the maximum out-of-plane displacement is about 38mm at the ultimate state. The von Mises stress distribution at the ultimate state indicates that some portions of the SCSW are yielded along its diagonal region; when the lateral deformation increases to the final state, the yield region continuously expands. In either the ultimate or final state, the yield portions of the SCSW are formed due to external shear loads, which are quite different from the diagonally continuous tension field in SPSW subjected to shear loads.

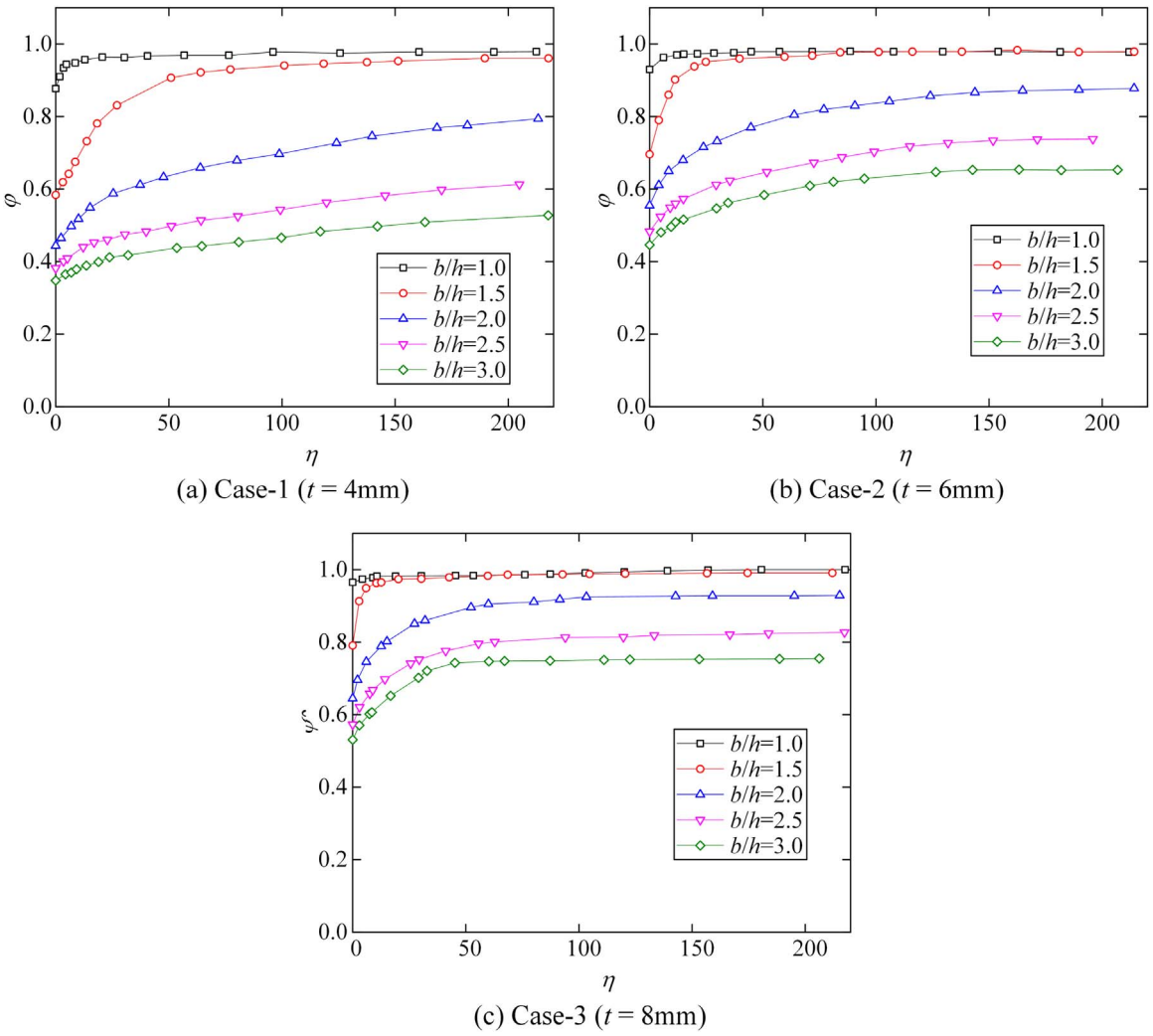

Fig. 15. Relationship between reduction factor and rigidity ratio.

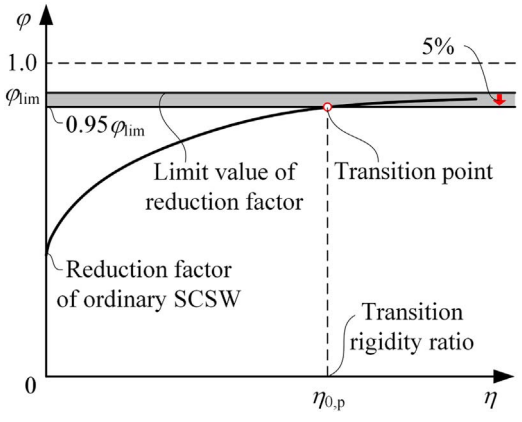

Fig. 16. Transition rigidity ratio of SSCSWs under elastoplastic analyses.

As shown in Fig. 13, a model with $\eta = 63.9$ is involved and the bucking wave is still diagonally across the whole plate, yet the maximum out-of-plane displacement is about 22mm at the ultimate state. It indicates that the out-of-plane displacements of the SCSW could be remarkably reduced by adding stiffening system to it. In addition, the von Mises distribution of the stiffeners is also depicted and it is observed that for both the ultimate and final states, most portions of the stiffeners remain elastic except some local regions at the bolted locations. It means that the stiffeners with Q345 material [22] are reasonable for the applications in SSCSWs.

As shown in Fig. 14, a model with $\eta = 213.2$ is presented, and the stiffening rigidity could be regarded as large enough to fully restrain the out-of-plane displacements of the corrugated plate at bolted locations. It is observed that the buckling wave of the SSCSW is evidently divided by the stiffening system into two parts, and the maximum out-of-plane displacement at the ultimate state is about 15mm. Similarly, the von Mises stress distribution of the stiffeners indicates that the stiffeners could remain elastic during the whole loading process.

4.2. Transition rigidity ratio under elastoplastic analyses

The shear resistance could be presented by the ultimate shear stress of the SSCSWs, τ_u, and a reduction factor of the shear stress, denoted by φ, could be defined as

$$\varphi = \frac{\tau_u}{\tau_y} \tag{11}$$

Fig. 15 presents the relationships between reduction factor φ and rigidity ratio η of different cases of numerical models, as tabulated in Table 1. It is observed that for each group of SSCSW models with the same aspect ratio and thickness, φ would increase with the increase of η. In addition, for each of the model group, when η gets large enough, the values of φ would tend to a limit value, which corresponds to the situation that the out-of-plane displacements of the corrugated wall are

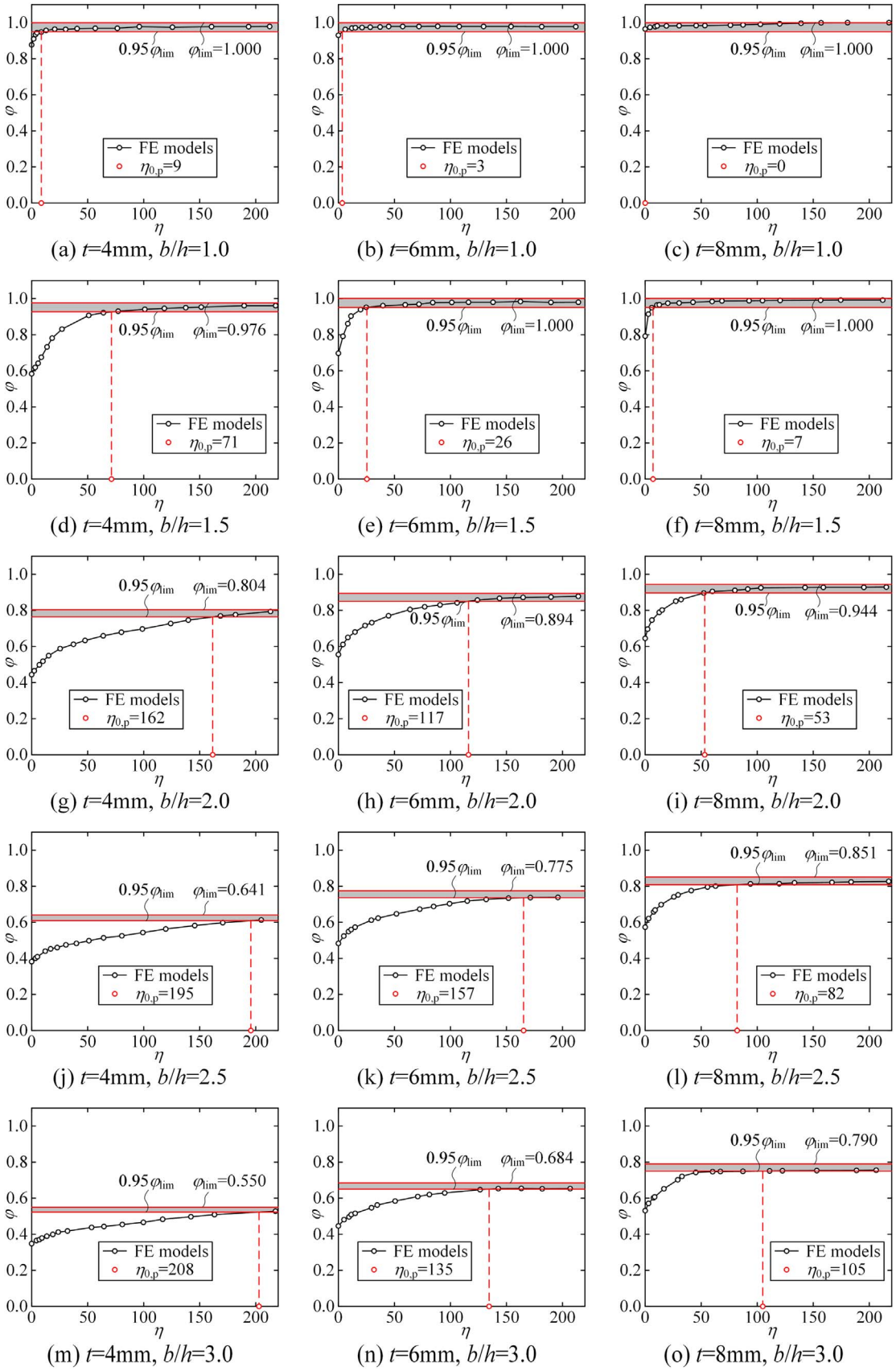

Fig. 17. Transition rigidity ratios of numerical cases.

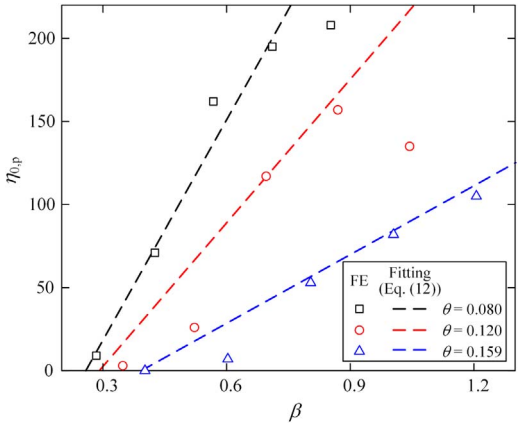

Fig. 18. Comparison of FE results and fitting formula.

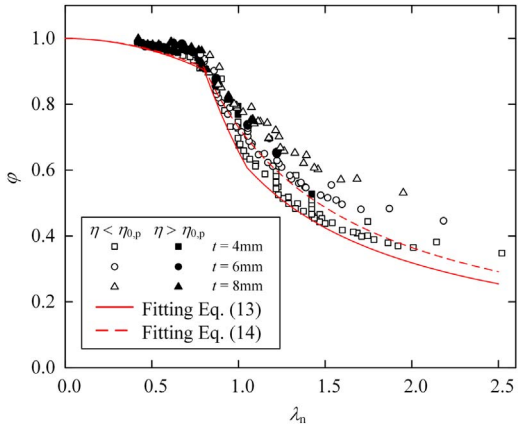

Fig. 19. Shear buckling curve of the SSCSWs.

fully restrained at the bolted locations. This value could be regarded as the upper limit of the reduction factor, which is denoted by φ_{lim}. Similar to the elastic buckling situations, a transition rigidity ratio under elastoplastic analyses is proposed to reflect approximately the critical rigidity ratio corresponding to the situation that adequate out-of-plane constraints are provided by the stiffening system. As shown in Fig. 16, since the reduction factors of SSCSWs with finite flexural rigidities of stiffening systems would not reach the upper limit φ_{lim}, adequate out-of-plane constraints are assumed to be provided when the reduction factor φ of the SSCSW exceeds 95% of φ_{lim}, and the η value corresponding to the transition point is defined as the transition rigidity ratio under elastoplastic analyses, denoted by $\eta_{0,p}$. If the bound is taken as a larger value (e.g. percentage > 98%), the material utilization and consumption in stiffeners would significantly increase, yet little increase of shear resistance is exhibited by the corrugated plate. On the other hand, if the bound is taken as a smaller value (e.g. percentage < 90%), limited material utilization and consumption is saved in the stiffeners, however, the shear resistance of the corrugated plate is over-reduced. In these considerations, a 95% bound is decided based on the efficiency of the material utilization of stiffeners, and it is regarded appropriate.

In order to obtain the upper limit of the reduction factor φ_{lim} of each model group, the FE model described by Fig. 10 is slightly adjusted by adding displacement constraints in y-direction (perpendicular to the plate) at each of the bolted locations, to simulate the stiffening system with infinite rigidity that could fully restrain the out-of-plane displacements of the corrugated plate. The obtained φ_{lim} values of all the FE model groups are tabulated in Table 1.

Based on the definition of $\eta_{0,p}$ and the obtained φ_{lim} values of all the FE model groups, the φ versus η curves of each model group are presented in Fig. 17, together with the φ_{lim} and $0.95\varphi_{lim}$ values. Accordingly, the transition rigidity ratios, $\eta_{0,p}$, of the FE model groups are obtained, which is also depicted in Fig. 17 and tabulated in Table 1.

It is observed that the value of $\eta_{0,p}$ decreases with the increase of the corrugated plate thickness t; while the value of $\eta_{0,p}$ increases with the increase of the aspect ratio of the corrugated plate b/h. In order to provide references to the engineers for practical design of SSCSWs, by using the numerical fitting technique, formula of $\eta_{0,p}$ is presented as Eq. (12) in terms of the design parameters of equivalent orthotropic plate of θ and β.

$$\eta_{0,p} = (750 - 3850\theta)\cdot\beta + 760\theta - 175 \tag{12}$$

The fitting formula of transition rigidity ratio $\eta_{0,p}$ is compared with the obtained $\eta_{0,p}$ values from FE analyses, as shown in Fig. 18. It is seen that the fitting formula of Eq. (12) could conservatively predict the transition rigidity ratios obtained from FE analyses for the parameter range of $0.08 < \theta < 0.16$. As mentioned that the transition rigidity ratio obtained from elastic buckling analyses could be approximately regarded as a constant value of $\eta_{0,e} = 100$ [7]. However, it is quite different for the elastoplastic situations as the transition rigidity ratios under elastoplastic analyses distribute in a quite wide range, which could be calculated from Eq. (12). In practical design, if the rigidity ratio of the SSCSW exceeds the transition value, a continuous increase of the stiffening rigidity would hardly improve the shear resistance of the SSCSW, yet it might continuously improve the ductile performance of the SSCSW.

4.3. Shear buckling curves

In order to provide a design method to predict the shear ultimate stress of the SSCSWs, shear buckling curves are proposed based on over 300 numerical points and by utilizing the numerical fitting technique. As shown in Eqs. (13) and (14), the shear buckling curves are expressed as the relationship between φ and λ_n.

$$\varphi = \begin{cases} 1 - 0.148\lambda_n^2 & \lambda_n \le 0.8 \\ [\Phi - \sqrt{\Phi^2 - 4\lambda_n^2}]/2\lambda_n^2 & 0.8 < \lambda_n \le 1.05 \\ 0.637/\lambda_n^{0.6} & \lambda_n > 1.05 \end{cases} \tag{13}$$

$$\varphi = \begin{cases} 1 - 0.137\lambda_n^2 & \lambda_n \le 0.8 \\ 0.73/\lambda_n & \lambda_n > 0.8 \end{cases} \tag{14}$$

in which Eq. (13) could be utilized in design of SSCSWs that $\eta \le \eta_{0,p}$, while Eq. (14) could be utilized in design of SSCSWs that $\eta > \eta_{0,p}$; the intermediate variable of Φ is expressed by Eq. (15).

$$\Phi = 0.5 + 0.68\lambda_n + \lambda_n^2 \tag{15}$$

The shear buckling curves are compared with the FE numerical results, as depicted in Fig. 19. The hollow symbols represent the models whose rigidity ratios are less than the transition value, while the solid symbols represent the models whose rigidity ratios are greater than the transition value. It is observed that the fitting formulas of Eqs. (13) and (14) could be utilized to conservatively predict the shear resistance of SSCSWs with $\eta \le \eta_{0,p}$ and $\eta > \eta_{0,p}$ respectively.

4.4. Design recommendations

Based on the FE numerical results on the shear resistant behavior of SSCSWs, the following design recommendations are provided for practical design of SSCSWs.

(1) It is recommended that the strength of the stiffeners is selected to be greater than the corrugated plate (e.g. Q235 material for the corrugated plate, while Q345 material for the stiffeners) for a more safe design where the failure of the stiffeners does not occur before the failure of the whole SSCSW. Yet this criterion could not fully

guarantee the safety of the stiffeners, and more detailed recommendations should be provided based on specific investigations of strength design of stiffeners. These strength requirements for designing stiffeners should be provided by further investigating the failure of stiffeners by considering their material nonlinearity, flexural-torsional deformation conditions and the interactions between the stiffeners and corrugated plate. However, this aspect if out of the major concern of this paper and needs further investigation.

(2) If the SSCSW is intended to be designed as inadequately restrained, i.e. $\eta \leq \eta_{0,p}$, its design should be based on the following Eq. (16).

$$V < \varphi\tau_y \cdot tb \tag{16}$$

in which V is the laterally external shear load; φ is the reduction factor and should be calculated based on Eq. (13).

(3) If the SSCSW is intended to be designed as adequately restrained, i.e. $\eta > \eta_{0,p}$, the sectional dimensions of the stiffeners should be selected based on the $\eta_{0,p}$ value, which could be calculated based on Eq. (12), and the design of SSCSW should also be based on Eq. (16), yet the reduction factor φ should be calculated based on Eq. (14).

(4) The SSCSW with its $\eta = \eta_{0,p}$ seems to be an economic design, since the continuous increase of the rigidity ratio would not further improve its ultimate resistance significantly. However, if the ductile performance of SSCSW is required, one could design the stiffeners with larger rigidity such that $\eta > \eta_{0,p}$ to further improve the ductility of the SSCSW.

5. Conclusion

In this paper, shear resistant behavior of stiffened steel corrugated shear walls (SSCSWs) is investigated via FE analyses considering both the geometrical and material nonlinearities, and the following conclusions can be drawn:

(1) The shear resistant behavior of SSCSWs with different stiffening rigidities are compared, which indicates that the stiffening system can effectively restrain the out-of-plane displacements of the corrugated wall, and can improve both shear resistance and ductility of the SSCSWs. Yet in this paper, due to lack of detailed design criterion of stiffeners, it is not guaranteed that the failure of stiffeners occurs before the failure of corrugated plate. This aspect is of significance for a comprehensive design of the SSCSWs and needs further investigation.

(2) For the SSCSWs with a parameter range of $0.08 < \theta < 0.16$, their transition rigidity ratio is defined and calculated based on FE results, and corresponding fitting formula is provided to conservatively predict the transition rigidity ratio values under elastoplastic analyses. Different from the constant transition rigidity ratio for elastic buckling situation, the provided transition rigidity ratio values under elastoplastic analyses distribute in a quite wide range.

(3) For the SSCSWs with a parameter range of $0.08 < \theta < 0.16$, two types of shear buckling formulas are fitted, and they are validated to be able to conservatively predict the ultimate shear stress of SSCSWs with $\eta \leq \eta_{0,p}$ and $\eta > \eta_{0,p}$ respectively. Accordingly, some design recommendations are provided for practical design of SSCSWs.

Acknowledgements

This study has been supported by research grants from the National Key R&D Program of China (No. 2016YFC0701201 and 2016YFC0701204).

References

[1] X. Zhang, Y. Guo, Behavior of steel plate shear walls with pre-compression adjacent frame columns, Thin Wall Struct. 77 (2014) 17–25.
[2] J. Berman, O. Celik, M. Bruneau, Comparing hysteretic behavior of light-gauge, steel plate shear walls and braced frames, Eng. Struct. 27 (2005) 475–485.
[3] J. Berman, M. Bruneau, Experimental investigation of light-gauge steel plate shear walls, J. Struct. Eng.-ASCE 131 (2005) 259–267.
[4] F. Emami, M. Mofid, A. Vafai, Experimental study on cyclic behavior of trapezoidally corrugated steel shear walls, Eng. Struct. 48 (2013) 750–762.
[5] F. Emami, M. Mofid, On the hysteretic behavior of trapezoidally corrugated steel shear walls, Struct. Des. Tall. Spec. 23 (2014) 94–104.
[6] H. Kalali, M. Hajsadeghi, T. Zirakian, F. Alaee, Hysteretic performance of SPSWs with trapezoidally horizontal corrugated web-plates, Steel Compos. Struct. 19 (2015) 277–292.
[7] J. Tong, Y. Guo, Elastic buckling behavior of steel trapezoidal corrugated shear walls with vertical stiffeners, Thin Wall Struct. 95 (2015) 31–39.
[8] L. Vigh, G. Deierlein, E. Miranda, A. Liel, S. Tipping, Seismic performance assessment of steel corrugated shear wall system using non-linear analysis, J. Constr Steel Res. 85 (2013) 48–59.
[9] N. Shimizu, R. Kanno, K. Ikarashi, K. Sato, K. Hanya, Cyclic behavior of corrugated steel shear diaphragms with end failure, J. Struct. Eng.-ASCE 139 (2013) 796–806.
[10] L. Vigh, A. Liel, G. Deierlein, E. Miranda, S. Tipping, Component model calibration for cyclic behavior of a corrugated shear wall, Thin Wall Struct. 75 (2014) 53–62.
[11] A. Farzampour, J. Laman, Behavior prediction of corrugated steel plate shear walls with openings, J. Constr. Steel Res. 114 (2015) 258–268.
[12] C. Yu, G. Yu, Experimental investigation of cold-formed steel framed shear wall using corrugated steel sheathing with circular holes, J. Struct. Eng.-ASCE 142 (2016).
[13] N. Feng, P. Cao, K. Wu, P. Zhang, Experimental investigation on strengthening of infilled frame structures by profiled steel sheet shear walls, Adv. Struct. Eng. 19 (2016) 703–714.
[14] M. Bahrebar, M. Kabir, T. Zirakian, M. Hajsadeghi, J. Lim, Structural performance assessment of trapezoidally-corrugated and centrally-perforated steel plate shear walls, J. Constr. Steel Res. 122 (2016) 584–594.
[15] M. Bahrebar, M. Kabir, M. Hajsadeghi, T. Zirakian, J. Lim, Structural performance of steel plate shear walls with trapezoidal corrugations and centrally-placed square perforations, Int. J. Steel Struct. 16 (2016) 845–855.
[16] W. Zhang, M. Mahdavian, Y. Li, C. Yu, Experiments and simulations of cold-formed steel wall assemblies using corrugated steel sheathing subjected to shear and gravity loads, J. Struct. Eng.-ASCE 143 (2017).
[17] J.T. Easley, D.E. Mcfarland, Buckling of light-gage corrugated metal shear diaphragms, J. Struct. Div. 95 (1969) 1497–1516.
[18] J.T. Easley, Buckling formulas for corrugated metal shear diaphragms, J. Struct. Div. 101 (1975) 1403–1417.
[19] T. Guo, R. Sause, Analysis of local elastic shear buckling of trapezoidal corrugated steel webs, J. Constr. Steel Res. 102 (2014) 59–71.
[20] C. Dou, Z. Jiang, Y. Pi, Y. Guo, Elastic shear buckling of sinusoidally corrugated steel plate shear wall, Eng. Struct. 121 (2016) 136–146.
[21] L. Hosseinzadeh, M. Mofid, A. Aziminejad, F. Emami, Elastic interactive buckling strength of corrugated steel shear wall under pure shear force, Struct. Des. Tall. Spec. 26 (2017).
[22] GB, Code for Design of Steel Structures. GB50017-2003, China Plan Publishing Company, Beijing, 2003.
[23] Y. Guo, Numerical and Experimental Investigations of Corrugated Steel Plate Composite Structures, Tsinghua University, Beijing, 2017.